
Benchmarking Deep Learning Models for Raman Spectroscopy Across Open-Source Datasets

Adithya Sineesh^{1*} Akshita Kamsali¹

¹Purdue University, West Lafayette

{asineesh, akamsali}@purdue.edu

Abstract

Deep learning classifiers for Raman spectroscopy are increasingly reported to outperform classical chemometric approaches. However their evaluations are often conducted in isolation or compared against traditional machine learning methods or trivially adapted vision-based architectures that were not originally proposed for Raman spectroscopy. As a result, direct comparisons between existing deep learning models developed specifically for Raman spectral analysis on shared open-source datasets remain scarce. To the best of our knowledge, this study presents one of the first systematic benchmarks comparing three or more published Raman-specific deep learning classifiers across multiple open-source Raman datasets. We evaluate five representative deep learning architectures under a unified training and hyperparameter tuning protocol across three open-source Raman datasets selected to support standard evaluation, fine-tuning, and explicit distribution-shift testing. We report classification accuracies and macro-averaged F1 scores to provide a fair and reproducible comparison of deep learning models for Raman spectra based classification.

1 Introduction

Raman spectroscopy is a non-destructive characterization technique, where the spectra encode vibrational signatures of molecular bonds. This non-destructive capability enables applications spanning biomedical diagnostics, pharmaceuticals, materials identification, food quality assessment and forensic analysis. Despite this breadth, Raman spectra are a weak scattering phenomenon, which leads to captured spectra often containing artifacts such as distortion by noise, background fluorescence, cosmic ray impacts and other environmental factors. These artifacts can dominate the class distinguishing features in the signal which complicates statistical learning for material identification [51]. Another challenge for automated identification of materials is the spectral overlap of the characteristic peaks of different components in the substance. Beyond additive noise, Raman spectra vary across systems and their configurations, acquisition times and strategies. Such heterogeneity can lead to significant distributional shifts, undermining the performance guarantees established on the test datasets when the models are deployed in the real world. At the same time, constructing large, labeled Raman spectroscopy datasets is costly as hardware is expensive and careful sample preparation, calibration and repeated measurements are labor intensive. Furthermore, annotation and assigning peaks to specific bonds or chemical groups often requires domain expertise which is often not available at scale. Machine Learning has therefore been increasingly adopted for material identification. Early works showcased the effectiveness of traditional chemometric approaches like Principal Component Analysis (PCA), Linear Discriminant Analysis (LDA) and Support Vector Machines (SVMs). More recent approaches leverage deep neural models, particularly one-dimensional convolutional networks [29] [5] [19] and attention-based architectures [28] [53]

*Corresponding author.

[21] and often report substantial gains over classical baselines. However, most of the existing works do not compare their proposed methods against other published deep learning approaches for Raman spectra classification.

Benchmarking under a standard evaluation framework allows for fair and meaningful comparisons across different architectures and algorithms. Such systematic evaluations help researchers identify which strategies are effective across different datasets and problem settings. These established reference points can serve as an excellent starting point for advancing state-of-the-art performance. In this work, we benchmark five deep learning models proposed for Raman spectra classification under a controlled and reproducible training and evaluation protocol across three open-source Raman datasets and report their accuracy and macro-averaged F1 score. We outline the motivation behind the selection along with the details of the models and the datasets in the subsequent sections.

2 Literature Survey

Machine learning techniques have been widely used for multi-class classification, where each spectrum is assigned to exactly one material. It has also been applied to the broader problem of multi-label classification, where the constraint of a sample containing only one target is relaxed. This task involves associating each Raman spectrum with multiple materials simultaneously. Multi-label classification with material concentration estimation further extends this task by estimating the mixing ratios in addition to predicting the components present in the sample. In the following subsections, we review the prior work in all these different types of Raman spectra classification. We organize the literature from foundational statistical approaches to modern deep learning based models.

2.1 Classic Chemometrics

Early Raman-based classification pipelines used linear dimensionality reduction to compress the spectrum and then trained shallow discriminative models with limited number of samples. For example, Rebrošová et al. categorized staphylococci into 16 strains using Principal Component Analysis (PCA) for feature compression followed by 1-NN classification on 277 spectra with 5-fold cross-validation [41]. Similarly, Monavar et al. leveraged PCA-derived representations with shallow Artificial Neural Networks (ANNs) and Linear Discriminant Analysis (LDA) for caviar type identification despite having only 93 spectra [33]. In pharmaceuticals, Roggo et al. used Support Vector Machine (SVM) based hierarchies to first identify tablet product families and then refine predictions to formulation categories via correlation-based methods and additional SVMs, using 25 product families comprising of 44 formulations (15 spectra per formulation) [43] in total. Generally, these classic chemometrics studies used compressed feature spaces coupled with lightweight classifiers. Recent years have seen a gradual shift from such traditional pipelines toward modern deep learning approaches that aim to learn representations directly from raw (or minimally processed) spectra and better tolerate perturbations expected in Raman spectra.

2.2 Deep Learning Models Evaluated on Small Experimental Raman Datasets

Deep Learning approaches for Raman spectroscopy mainly involve developing 1-D Convolutional Neural Networks (CNNs) or transformers and comparing them against classical baselines. An early example is the Deep CNN mineral classifier by Liu et al. [29], which was evaluated against KNN/SVM/Random Forest on RRUFF-derived datasets [23]. While such studies established the potential of CNN-based models for Raman analysis, their evaluations were often conducted on test sets comprising of a limited number of experimentally acquired spectra. For example, Dong et al. designed a CNN with constrained kernels that emulate standard denoising and baseline-correction operations. The model achieved superior binary classification of human vs. animal blood (109 test spectra spanning humans, dogs, and rabbits using a 67:33 train-test split), outperforming SVM and PLS-DA [5]. Similarly, Kirchberger-Tolstik et al. developed a CNN model to predict the severity of Ulcerative Colitis using the Raman spectra of the colon biopsy [19]. The model was assessed using patient level cross-validation on 227 Raman spectra acquired from 42 patients and not compared with any other approaches.

A Locally Connected Neural Network (LCNN) designed by Houston et al. [16] was used to detect chlorinated solvents using the Raman spectra of the samples. Despite outperforming SVM, KNN,

Decision Tree, Gaussian Naive Bayes and Fully Connected Neural Network (FCNN), the evaluation was performed on a small real dataset of 58 test spectra. In another example, the classification of three marine pathogen strains was achieved with the help of Generative Adversarial Networks [56] by Yu et al. The independent Generator-Discriminator for each pathogen strain were trained on the corresponding 50 experimental spectra. Testing was conducted on 60 real spectra, achieving a reported 100% classification accuracy, though the method was not compared against competing approaches.

RaMixNet I and II [34] were developed for multi-label material identification and multi-label classification with concentration estimation respectively. These models were trained primarily on synthetic spectra generated by linear combinations of four pure compounds with additional baseline drift and spectral augmentations. Evaluation on real data was restricted to only six experimentally measured mixtures where they outperformed correlation-based methods and Partial Least Squares Regression.

While these works showed the promising performance of deep learning methods, their heavy reliance on small-scaled experimental datasets raises questions about their efficacy during real-world deployment.

2.3 Synthetic Data Driven Evaluation of Raman Classification Models

Subsequent works tried to alleviate the limitation of small-scaled experimental datasets by making extensive use of synthetic data. For example, Qi et al. developed a CNN model to classify 10 different 2-D materials [39] like Graphene using limited number of real Raman spectra along with large quantities of synthetic data generated by Denoising Diffusion Probabilistic Models (DDPMs) [15]. The dataset consisted of 10,000 synthetic spectra and 594 experimental spectra. The authors compared their model to SVM, ANN, KNN methods using a 10 fold cross-validation scheme. Similarly, Hamed Mozaffari and Tay trained a model consisting of a single 1-D convolutional layer with two linear layers [35] on 40,000 synthetic spectra generated by augmenting 5 real Raman spectra of 5 different materials. This model outperformed several other published Raman ML models on this 5-category classification problem. However, the test dataset comprised of 5000 synthetic spectra generated by augmenting the same 5 gold-standard spectra as the train dataset.

DeepCID [10] further exemplifies this evaluation protocol. The framework is comprised of a suite of CNN models that each predict if a specific material is present in the sample or not. The models are trained on synthetically generated spectra that were generated by applying augmentations to 167 real spectra of pure common pharmaceutical raw materials. It outperforms traditional chemometric methods and a FCNN on synthetic data and limited real Raman spectra of mixtures. Overall, synthetic data is often used as a remedy for the scarcity of experimentally acquired Raman spectra. But evaluating models on synthetic test datasets leads to the same limitations of using small real test datasets i.e. uncertainty about their performance on unseen samples during real-world deployment.

2.4 Evaluation Limited to Classical or Generic Deep Learning Baselines

In addition to the limitations due to the use of small experimental or synthetic test datasets, several deep learning models for Raman spectroscopy have been proposed without systematic comparison to existing Raman-specific deep learning approaches. Evaluations are often restricted to classical machine-learning baselines or generic image-based architectures which makes it difficult to assess the merits of the proposed methods within the broader Raman spectroscopy literature. For example, Maruthamuthu et al. used a ResNet-18 [13] inspired CNN model for the detection of microbial contamination [32]. The dataset contained 6000 real Raman spectra each of Chinese Hamster Ovary (CHO) cells, which are widely used in the pharmaceutical industry, along with 12 microbes that are the common contaminants of CHO and 3 mixtures of CHO and contaminant microbes. The model was trained using a 5-fold cross-validation scheme but not compared against any other approaches, and the exhaustive dataset is not public.

Similarly, Primrose et al. adapted the VGG13 [44] architecture for Raman spectra classification by replacing all the 2-D convolutional layers with 1-D convolutional layers [37]. This model was then trained on a synthetically mixed dataset and was evaluated on limited data collected by the First Defender Raman spectrometer and showed >90% detection rates for certain explosive materials and their precursors, outperforming the algorithm used by the spectrometer. This work was extended

[38] to include additional non-explosive materials and the evaluation was performed over 10,000 real Raman spectra but the dataset was not made public and the model was not compared against other published Raman-specific approaches.

A similar evaluation pattern is observed for Raman Spectral Translation (RST) [53], which was developed for multi-label classification by combining the ideas from CNNs and transformers. However, the comparisons were limited to a generic CNN and DenseNet [17], rather than against established Raman-domain architectures, on a real test dataset. Likewise, a transformer model for classification of deep-sea cold seep bacteria [28] and a CNN model for classification of plastics [40] were compared using experimental test spectra against 1-D variants of AlexNet [22], ResNet and SVM, LDA and Decision Trees respectively.

This trend extends to biomedical and agricultural applications as well. The RFBC [3] model used a hybrid CNN-LSTM architecture incorporating Fourier-domain features and outperformed PCA-SVM, PCA-KNN and PCA-XGBoost in detecting different brands of rice on a test dataset containing experimental Raman spectra. Similarly, Y. Lin et al. developed a ResNet-18 based model for cancer detection [27] using 2-D transforms of 1-D serum Raman spectra (CWT/heatmaps). The authors evaluated the model only against generic image classifiers like AlexNet, VGG16, DenseNet. Kok et al. designed another ResNet-based model, with multi-channel inputs spanning raw spectra plus multiple pre-processed views, [20] for osteoarthritis cartilage classification and compared the model against baseline CNNs. Similarly, Ullah et al. developed a Multi-Layer Perceptron (MLP) to detect tuberculosis from blood serum samples [48] but did not compare the model with any other approaches.

Du et al. developed another shallow CNN to classify *Bacillus* spores [7] but only compared the model to traditional ML approaches like SVM. RaT and RaST were transformer and Swin-Transformer [31] based architectures proposed for classifying lactic acid bacteria into 14 different strains [52]. These models were evaluated on an experimental test dataset against an adapted ResNet model, SVM, LDA, KNN and XGBoost.

Likewise, the evaluation is restricted to MLP, Least squares, modified VGG11 and ResNet-50 for the RamanFormer [21], which was proposed to quantify the presence of Methanol, Isopropyl Alcohol and Ethanolamine in the Raman spectra of the mixture. Another example is ConInceDeep [58], a multi-label classification model that combines Continuous Wavelet Transform (CWT) representations with convolution-based Inception Modules [47]. It was evaluated against ablated variants of its own proposed architecture.

Collectively, these works demonstrate a huge variety of deep learning approaches developed for Raman spectroscopy across different domains. However, the lack of systematic benchmarking against established Raman-specific models hampers the ability to draw meaningful conclusions across multiple papers.

2.5 Limited Benchmarking

Only a few works in Raman deep learning literature attempt explicit benchmarking against previously published models. However, the scope of the comparison is often limited in these cases.

RamanNet was proposed as a general Raman spectra classifier [18] and was evaluated on open-source datasets like the COVID-19 Raman dataset [55], Melanoma dataset [9], RRUFF Mineral database [23] and the Bacteria-ID dataset [14]. While RamanNet outperformed the baseline for each dataset, the benchmarking was limited as the comparison was just against one model per dataset. A Scale-Adaptive deep neural network (SANet) was designed for identifying the isolate and the empiric treatment for the sample based on its Raman spectrum [4]. The model was trained and evaluated on the Bacteria-ID dataset and compared against the model presented in that work [14] and traditional ML methods like SVM and Linear Regression rather than a broader set of Raman-specific deep learning models.

The Wavelet Packet transform and Gramian Angular field (WPGA) algorithm was developed by Liu et al. to generate 2-D spectrograms from 1-D Raman spectral data [30]. The authors then showed that a ResNet based model using these 2-D spectrograms outperformed several published Raman classifier models [14] [18] [59] on the open-source Bacteria-ID dataset [14]. However, the official implementation of the model is not publicly available, and the paper and its supplementary material

do not provide sufficient architectural details to allow for an exact reproduction of the proposed network.

Lange et al. published an open-source dataset containing 6960 Raman spectra of mixtures containing 8 different metabolites in varying concentrations [25]. The authors compared 11 different models on it but only one of those models was published for Raman spectra classification.

Overall, the prior work in Raman spectra classification shows tremendous architectural innovation but suffers from limitations due to: (i) small experimental datasets or synthetically generated test sets, (ii) comparisons restricted to classical machine-learning baselines or trivially adapted vision models. This complicates meaningful cross-paper performance assessment. In this work, we present systematic, reproducible benchmarking under consistent experimental settings for five deep learning models across three open-source Raman spectral datasets.

3 Benchmark Models

In the previous section, we highlighted the numerous approaches employed over the years for material classification and material analysis of samples based on their Raman spectrum. In this work, the benchmarking is limited to just Deep Learning models for multi-class classification. We chose five models, detailed in subsequent sections, which represent a variety of architectural designs, complexities and sizes as shown in Table 1. All these models were trained using Cross-Entropy Loss, unless mentioned otherwise.

Table 1: The five chosen models in terms of parameter count and multiply-accumulate (MAC) operations for a Raman spectrum of length 1024 with 15 output classes.

Model	Number of parameters (M)	MACs (M)
Deep CNN [29]	15.91	21.77
SANet [4]	2.23	102.48
RamanNet [18]	0.72	0.72
Transformer [28]	85.17	769.88
RamanFormer [21]	4.31	24.33

3.1 CNN based models

The Deep CNN model [29] was one of the first Deep Learning models introduced for Raman spectra classification and is based on the famous LeNet-5 Architecture [26]. It consists of three 1-D convolutional layers with kernel sizes of 21, 11 and 5 interleaved with pooling layers that reduce the spatial dimension of the spectra. The features generated by these layers are then passed through a dense linear layer followed by a classification head, which contains the same number of output nodes as the number of classes in the dataset.

Convolution has the property of shift equivariance, which is desirable for images but detrimental for Raman spectra where the position of the peak plays a vital role in identifying the material. The RamanNet [18] model was developed to be free from this translational equivariance. The spectrum is split into overlapping sliding windows of a fixed size and each window is passed through its own multi-layer perceptron. This operation is similar to convolution but with different kernels applied to different spatial locations. The outputs for all the windows are then concatenated and passed through another multi-layer perceptron and a linear embedding layer to obtain the feature representation of the spectra. These features are then fed into a classification head to obtain the predicted label. RamanNet is trained using a linear combination of triplet loss on the feature representation of the spectra and Cross-Entropy loss on the predicted class labels.

At each convolutional layer in a CNN, the size of the Receptive Field (RF) is constant. This property was said to be undesirable for capturing the peaks of a Raman spectrum, which are of different widths, and thus the Scale Adaptive Network (SANet) [4] was developed. It consists of five Multi-Scale Blocks for feature extraction with each Block consisting of six 1-D convolutional layers having increasing kernel sizes from 3 to 13. This allows for each Block to capture the features at different

scales of RF. These features are stacked along the channel dimension followed by channel-attention and point-wise convolution to extract only the relevant features while reducing the channel dimension. The features generated by the sequence of MultiScale Blocks are then flattened and passed through the classification head.

3.2 Transformer based models

Recent years have seen the proliferation of attention-based mechanisms for vision and language tasks. The transformer[50] architecture, which is solely based on attention, has also been adopted for the classification of Raman spectra. This development was only natural as the attention mechanism of the transformer was originally designed to model sequential data. The earliest such attempt involved simply adapting the Vision Transformer (ViT)[6] for the 1-D spectral domain [28]. The spectrum is split into patches and then passed through a linear layer to map them to tokens of dimension 768. A learnable class token of the same dimension is appended to this sequence of tokens followed by the addition of Position encoding to track the sequence of tokens. The model consists of 12 transformer blocks, each comprising of a 12-head self-attention layer and a multi-layer perceptron. The former captures the relationships between the different tokens in the sequence and the latter helps to generate higher-level features from each token. At the output of the transformer blocks, the embedding of the class token serves as the aggregate representation of the input sequence. Therefore, this embedding is passed through the classification head. This model shall be referred to as the Transformer in the subsequent sections.

The RamanFormer [21] further modifies the transformer architecture for processing Raman spectra. The generation of tokens from the spectrum remains the same, only without the class token and with a reduced embedding dimension of 256. This sequence of 8 tokens are passed through just three transformer blocks, each containing a 8-head self-attention layer and a MLP. The output token sequence is fed through two strided convolutional layers to capture the spatial hierarchy. The features are the pooled along the temporal dimension followed by passing them through a dense layer and classification head. Although RamanFormer was originally proposed for Mixture analysis of Raman spectra, we use it for classification tasks. The underlying architecture remains the same with Cross-Entropy loss being used instead of the original L1 loss.

4 Datasets

We surveyed publicly available Raman spectroscopy datasets and selected three that span distinct application domains and exhibit varying degrees of distribution shift between the training and test sets. Specifically, we choose the MLROD (minerals) [1], Bacteria-ID [14] (biomedical), and API [11] (pharmaceutical) datasets as shown in Figure 1. The MLROD test set was generated under different conditions than the training set, enabling evaluation under distribution shift. The Bacteria-ID dataset consists of a reference set suitable for pretraining and a smaller fine-tuning set that contains the same degradation in optical system efficiency as the test dataset. Meanwhile the test split of the API dataset is from the same distribution as the train and validation split. However, unlike the previously mentioned datasets, the API dataset does not provide predefined train and test splits and these splits must be constructed by the user. We now discuss the three datasets and its corresponding acquisition method and the criteria we test for.

Machine Learning Raman Open Dataset (MLROD) MLROD is a high-volume Raman dataset created for material detection on Mars. It contains 89,121 labeled spectra spanning 12 pure mineral classes and 3 binary 1:1 powder mixtures. Mineral classes are: Quartz, Albite, Anorthite, Microcline, Hornblende, Biotite, Muscovite, Forsterite, Augite, Enstatite, Calcite, Gypsum; mixtures are Quartz+Albite, Forsterite+Augite, Forsterite+Albite. It also consists of a separate set of test spectra (rocks, with and without dust): 39,720 spectra from Gabbro and Granite slabs, measured under clean (0% dust) and dusty (50% Basaltic dust coverage) conditions (e.g., Gabbro: 8,952 clean / 9,740 dusty; Granite: 11,028 and 10,000 across the two conditions as listed)². The “dusty” regime was created using basaltic dust to mimic the obscuration in Martian conditions. Figure 2 shows the difference in

²When we downloaded the data from the official website, the training dataset had 90,341 spectra. Several of the spectra in the Granite 50% dust test dataset have a label that does not correspond to any of the labels in the training dataset. We have ignored these samples for the purposes of evaluation and therefore the size of the Granite 50% dust test dataset is 5,183 and the size of the overall test dataset is 34,903.

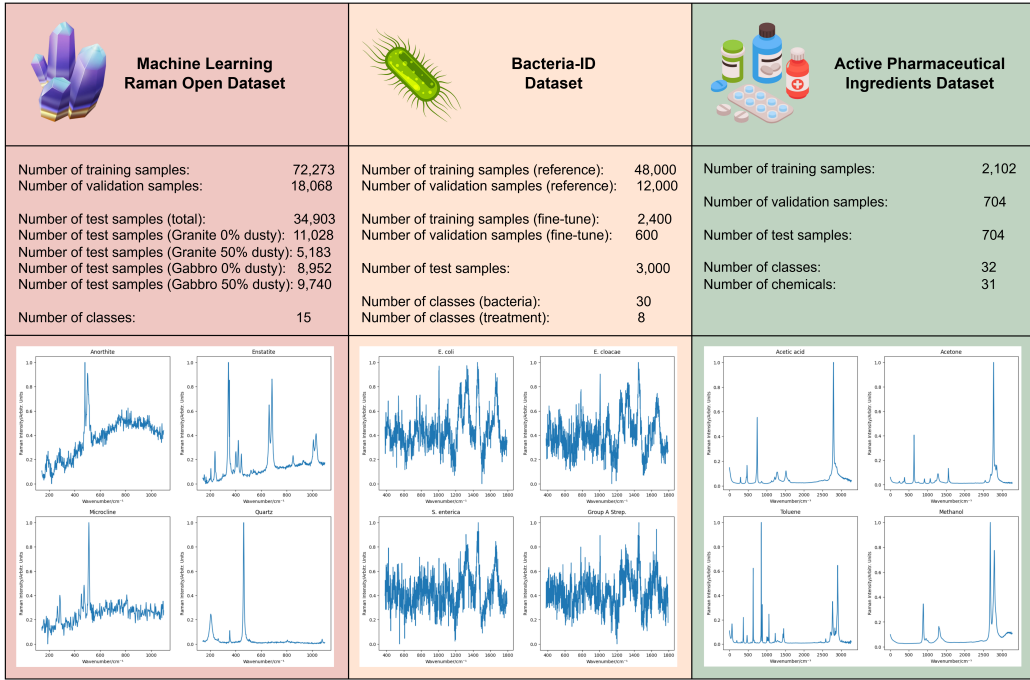


Figure 1: **Dataset overview and qualitative comparison across domains.** Top row: the three Raman spectroscopy datasets used in this study: 1. **MLROD** (mineral spectra), 2. **Bacteria-ID** (spectra of bacterial species/strains), and 3. **API** dataset (spectra of active pharmaceutical ingredients). Middle row: dataset-level statistics summarizing scale and label structure including total number of classes. Bottom row: **representative spectra** randomly sampled from each dataset (intensity vs. Raman shift (cm^{-1})).

the Raman spectra collected in the “train”, “clean” test and “dusty” test regimes. The dataset was collected on Horiba LabRAM HR Evolution single stage spectrometer with 532 nm excitation with no pre-processing steps and only standardizing the axis via interpolation and trimming.

Bacteria-ID Dataset It is a bacterial (mostly monolayer and single-cell) Raman spectroscopy dataset intended for pathogen identification and downstream grouping by 8 antibiotic treatments. The dataset provides a reference dataset across 30 bacterial plus yeast isolates with 2000 spectra per isolate for training. Additionally, it contains fine-tuning and test sets each with 100 spectra per isolate. The dataset was collected on Horiba LabRAM HR Evolution Raman microscope at 633nm excitation with polynomial background correction and per-spectrum min-max normalization to [0,1] range.

Active Pharmaceutical Ingredients (API) Dataset The API dataset is an open-source dataset with 3510 spectra spanning 32 pure compounds measured on Raman Rxn2 analyzer at 785nm excitation. The dataset provided comes with automatic instrument pre-treatment which includes dark noise subtraction, cosmic ray filtering and intensity correction with no other pre-processing steps.

5 Methodology

In this section, we outline the training methodology and evaluation approach used to benchmark the five deep learning models on the three open-source Raman spectroscopy datasets. For consistency, we use the same optimization procedure (Adam), model-selection criterion, and stopping rules across all models, while tuning hyperparameters independently for each dataset using an identical search procedure.

Preprocessing For all datasets, we applied only intensity scaling to the raw spectra to improve the numerical stability of the convolution and attention-based models. We intentionally skip any further pre-processing steps such as baseline correction, fluorescence removal, scatter correction,

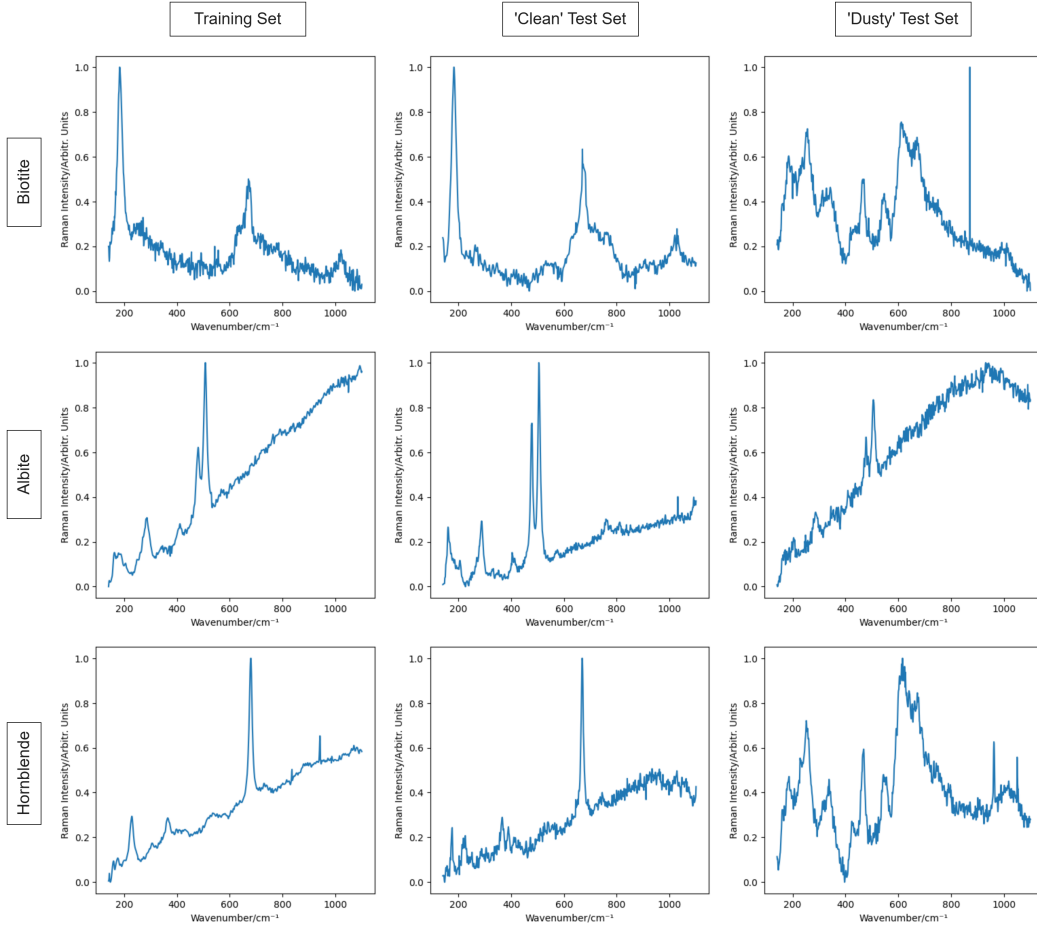


Figure 2: MLROD spectral shift across evaluation conditions (“clean” vs. “dusty”). Representative Raman spectra for three minerals (**Biotite**, **Albite**, **Hornblende**) shown across the **training set** (left), **‘clean’ test set** (middle), and **‘dusty test’ set** (right). Each row corresponds to the same material label across splits; each trace is a single example spectrum plotted as Raman intensity (arb. units) versus wavenumber (cm^{-1}). While the training and ‘clean’ test spectra largely preserve characteristic peak locations and relative band structure, the ‘dusty’ split exhibits pronounced contamination artifacts such as elevated and drifting baselines, broadened features, and spurious high-intensity components. This illustrates a significant distribution shift that challenges model generalization.

Table 2: List of hyperparameters evaluated for the grid search, applied independently to each of the five models on all three datasets, with separate tuning for every model–dataset pair to ensure fair comparisons.

Hyperparameters	Values
Batch Size	32, 128, 512
Learning Rate	1e-3, 1e-4, 1e-5

or denoising. Although several procedures exist for each of the processing steps, it is difficult to engineer an effective pre-processing pipeline that can be applied to all the datasets. This is because it is challenging to identify which combination of methods is optimal, as in most cases they lead to worse model performance [8]. Deep learning based approaches for artifact removal have also been developed recently [12] [45] but they add to the time complexity of the pre-processing pipeline and can obscure whether performance gains arise from the classifier architecture or from learnable pre-

processing. Our goal is to benchmark model behavior under a minimal, reproducible pre-processing regime.

Hyperparameter tuning and model selection For each model-dataset pair, we performed hyperparameter tuning via 3×3 grid search over the ranges listed in Table 2. We select the final model based on validation performance, and report test results using the checkpoint that achieves the best validation accuracy (early stopping). This tuning was performed independently per dataset to avoid transferring dataset-specific choices across domains.

MLROD We divided the MLROD training dataset into the train and validation datasets using a random 80:20 train-val split. The training was for up to 40 epochs, with early stopping applied if the validation accuracy didn't improve for 10 consecutive epochs. We then evaluated the model with the best validation accuracy on the hold-out test dataset. We also reported the accuracy separately for the clean Gabbro, clean Granite, dusty Gabbro and dusty Granite subsets of the test dataset.

Bacteria-ID The 3 relevant subsets used from the Bacteria-ID dataset to benchmark the selected models were the reference, fine-tune and test sets. We divided the reference and fine-tune sets into their corresponding train and validation datasets using a random 80:20 train-val split. The pretraining was for up to 40 epochs on the train split of the reference set, with early stopping applied if the accuracy did not improve on the validation split of the reference set for 10 consecutive epochs.

The model with the best reference validation accuracy was then trained on the fine-tune train split with a tenth of the learning rate used in pretraining. The fine-tuning was for up to 40 epochs with early stopping applied if the accuracy did not improve on the validation split of the fine-tune set for 10 consecutive epochs. We then reported the accuracy on the test set using the model with the best fine-tune validation accuracy. All the trained models were trained separately on the two tasks of classifying the isolate and classifying the empiric treatment.

API Dataset For the API dataset, we generated the validation and test splits by randomly sampling 22 disjoint samples each for all the 32 classes and assigned the remaining samples to the training set. This approach approximately corresponds to a 60:20:20 train-val-test split. We used the same train-val-test splits for the hyperparameter tuning and inference for all the models.

The training was capped at 40 epochs with early stopping if the validation accuracy of the model did not improve in the past 10 epochs. We then evaluated the model with the best validation accuracy on the test split.

Although the dataset contains 32 labeled compounds, two of them, 4-methyl-2-pentanone and methyl isobutyl ketone, are chemically identical³. This is also highlighted in the dataset, where the samples of both these compounds have highly similar Raman spectra, as shown in Figure 3. Therefore, we report the results under two evaluation protocols. First, a 32 class setting that follows the dataset labels. Second, a 31 class setting where these two labels are merged post-hoc during evaluation. All the models are trained under the 32 class problem.

Implementation Details All experiments were run on a server with an Intel Xeon CPU (3.0 GHz), 64 GB RAM, and an NVIDIA RTX A5000 GPU. All models were implemented in PyTorch, and the training scripts can be found at https://github.com/asineesh/Benchmark_Raman_DeepLearning/. SANet uses the authors' official PyTorch implementation, while the other models were reimplemented based on the details in the original papers or accompanying TensorFlow code.

6 Results

For all the five models, we report their performance across the three datasets using accuracy and macro-averaged F1 score in the following subsections. Accuracy provides a simple and intuitive measure of overall correctness across all the samples and it is defined as follows:

$$\text{Accuracy} = \frac{1}{N} \sum_{i=1}^N \mathbb{1}(\hat{y}_i = y_i) \quad (1)$$

³<https://pubchem.ncbi.nlm.nih.gov/compound/Methyl-Isobutyl-Ketone>

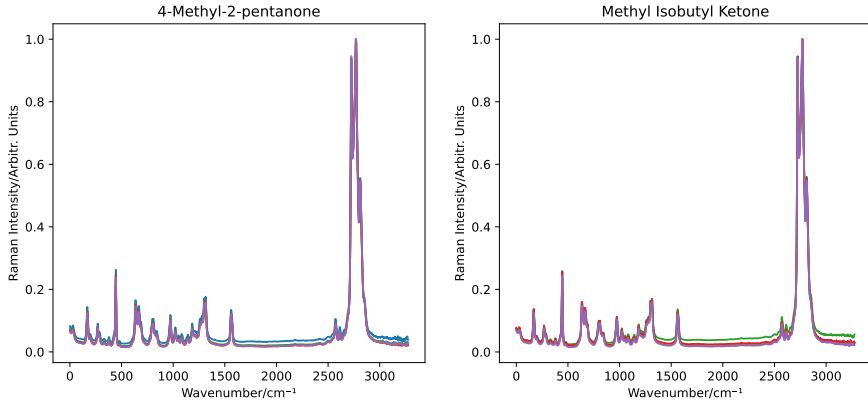


Figure 3: **API dataset label synonymy.** Overlaid Raman spectra (five randomly selected measurements per panel) for **4-methyl-2-pentanone** (left) and **methyl isobutyl ketone** (right), plotted as Raman intensity (arb. units) versus wavenumber (cm^{-1}). The near-identical signatures across the two panels reflect that methyl isobutyl ketone and 4-methyl-2-pentanone are chemically identical, illustrating potential label aliasing in the dataset and motivating label harmonization during our evaluation.

where N is the total number of samples, $\mathbb{1}()$ denotes the indicator function, y_i denotes the ground-truth class label and \hat{y}_i denotes the predicted class label for the i^{th} sample.

However, accuracy can be misleading in the presence of class imbalance. For example, strong performance on more frequent classes can mask poor performance on less frequent classes. To provide a more comprehensive and class-balanced assessment of model performance, we additionally report the macro-averaged F1 score.

The macro-averaged F1 score is the unweighted average of the F1 scores per class and is defined as follows:

$$\text{macro F1} = \frac{1}{C} \sum_{c=1}^C \text{F1}_c \quad (2)$$

where the F1 score per class is defined as

$$\text{F1}_c = \frac{2 * \text{TP}_c}{2 * \text{TP}_c + \text{FP}_c + \text{FN}_c} \quad (3)$$

where TP_c is the number of true positives, FN_c is the number of false negatives, and FP_c is the number of false positives for class c .

By reporting both accuracy and macro-averaged F1 score, we capture the overall classification performance while ensuring that performance on minority classes is not obscured by the majority classes.

6.1 MLROD

Table 3 shows the classification results for the five selected models trained and tested on the MLROD. As expected all the models perform substantially worse on the dusty samples, showcasing the sensitivity of these classifiers to interference. Since dust contaminated spectra are not part of the training dataset, this degradation in performance is due to distribution shift and not overfitting on the training dataset.

The SANet model showcases the best overall accuracy performance, over 5 percentage points higher than the worst model (Transformer). However upon further investigation, it was observed that all of these models achieve significantly higher validation accuracies than test accuracies. For example, SANet achieves a validation accuracy of 100%, which is 21 percentage points more than its

corresponding test accuracy. Similarly, the Deep CNN, RamanNet, Transformer and RamanFormer models achieve a 99.99%, 99.76%, 99.69% and 99.75% validation accuracies respectively, which are all considerably higher than their corresponding test accuracies.

Table 3: Test accuracy and F1 score of the chosen models on different subsets of the MLROD test dataset. The F1 score here refers to the macro-averaged F1 score. \uparrow indicates that higher values correspond to better performance for the reported metrics. Boldface highlights the best-performing model in each column.

Model	Granite 0% dusty		Granite 50% dusty		Gabbro 0% dusty		Gabbro 50% dusty		Overall	
	Accuracy \uparrow	F1 score \uparrow								
Deep CNN [29]	99.22%	0.6797	76.42%	0.3103	77.42%	0.7589	53.19%	0.2026	77.4%	0.7371
SANet [4]	92.85%	0.6713	80.69%	0.3311	91.13%	0.7874	52.15%	0.1756	79.25%	0.7038
RamanNet [18]	90.4%	0.4568	65.68%	0.2416	98.51%	0.5337	41.31%	0.167	75.11%	0.6592
Transformer [28]	90.76%	0.454	59.12%	0.2212	93.59%	0.4217	44.98%	0.1602	74.01%	0.5904
RamanFormer [21]	92.5%	0.5944	62.01%	0.2612	95.74%	0.4821	46.2%	0.169	75.88%	0.6759

This disparity between the accuracies on the test and validation dataset can be explained by the fact that the Raman spectra in the train and test datasets were collected separately from varying locations. In other words, the train and test samples are drawn from different distributions. Therefore, the reported test results are a reflection of model robustness under domain shift rather than in-distribution classification performance. The macro-averaged F1 score being significantly lower than the test accuracy across all the subsets of the MLROD test dataset means that one or more classes are performing considerably worse than the dominant classes.

6.2 Bacteria-ID

We report the classification results of the five selected models on two tasks: (1) classifying the isolate (2) classifying the empiric treatment in Table 4. For the first task, the Transformer performs the worst and classification accuracy of all the other trained models are within 2 percentage points of each other. This spread is narrower for the second task, with the test accuracies of the best and worst performing models being within 1 percentage point of each other. The comparable macro-averaged F1 score and test accuracy for all the models suggest balanced performance across the classes.

Table 4: Test accuracy and F1 score of the chosen models on the test dataset of the Bacteria-ID dataset. The F1 score here refers to the macro-averaged F1 score. \uparrow indicates that higher values correspond to better performance for the reported metrics. Boldface highlights the best-performing model in each column.

Model	30 isolates		8 treatments	
	Accuracy \uparrow	F1 score \uparrow	Accuracy \uparrow	F1 score \uparrow
Deep CNN [29]	85.8%	0.8559	97.63%	0.9804
SANet [4]	86.13%	0.8573	96.77%	0.9699
RamanNet [18]	83.67%	0.8348	96.87%	0.9711
Transformer [28]	81.53%	0.8093	96.63%	0.9676
RamanFormer [21]	84.23%	0.8376	97.1%	0.9752

6.3 API Dataset

We show the results of all the selected models on the 32 category classification task in the Dataset Label Space and the 31 category classification task in the Chemical Identity Space of the API dataset in Table 5. For the former, the Transformer is the worst performing model and the accuracy of the Deep CNN, RamanNet and RamanFormer are all within a percentage point of each other followed by the SANet being 2 percentage points clear from this pack. The macro-averaged F1 score being similar to the test accuracy is indicative of relatively uniform classification performance across the different categories for all the 5 models.

We observe a consistent increase in performance for the 31 category evaluation, with all the models except the Transformer achieving perfect test accuracy. This improvement across the models suggests

that most of the errors in the 32-class setting arise from confusion between synonymous labels rather than a failure to learn chemically meaningful representations.

Table 5: Test accuracy and F1 score of the chosen models on the test dataset of the API dataset. The F1 score here refers to the macro-averaged F1 score. \uparrow indicates that higher values correspond to better performance for the reported metrics. Boldface highlights the best-performing model in each column.

Model	Dataset Label Space		Chemical Identity Space	
	Accuracy \uparrow	F1 score \uparrow	Accuracy \uparrow	F1 score \uparrow
Deep CNN [29]	96.59%	0.9658	100.0%	1.0
SANet [4]	99.57%	0.9957	100.0%	1.0
RamanNet [18]	97.02%	0.9662	100.0%	1.0
Transformer [28]	95.74%	0.9492	98.86%	0.9882
RamanFormer [21]	97.3%	0.9683	100.0%	1.0

7 Discussions

Systematic benchmarking plays an important role in identifying the strengths and weaknesses of different approaches for a given problem. In this work, we compare the performance of five deep learning Raman models across three open-source Raman spectroscopy datasets under consistent training configurations. With this set-up, SANet demonstrates the strongest performance across the datasets. In contrast, the relative under-performance of the transformer-based models indicates that, despite their success in vision and language tasks, further architectural adaptations, training strategies or larger datasets may be required to unlock their full potential.

As shown in Table 3, variations in the spectroscopic hardware and acquisition set-up lead to covariate shifts in the Raman spectra captured in the train and test datasets. Calibration Transfer and Maintenance (CTM) methods in Chemometrics [36] can achieve adaptation between the source(train) and target(test) domains. Many of these CTM methods are not viable for the classification task in MLROD as they require labels for the samples in the target(test) domain [24] [2]. Recent works have proposed unsupervised domain adaptation frameworks [49] [57] but their effectiveness beyond the originally reported datasets are yet to be independently evaluated.

Another approach to solving this issue is by using self-supervised frameworks on large amounts of unlabeled data to learn more robust representations of Raman spectra. SMAE [42] employs a transformer-based encoder and decoder architecture where the self-supervised pretraining task involves recovering the original spectrum from a randomly masked spectrum. The effectiveness of the learned representations was showcased by achieving an unsupervised clustering accuracy of 80.56% for the 30 class pathogenic species identification problem, where K-means clustering was applied to the extracted features of the Raman spectra in the test set of the Bacteria-ID dataset. SemiRaman [46] is another framework that combines self-supervised contrastive learning with semi-supervised learning. It involves pretraining an encoder with several contrastive loss functions on augmented views of the same spectrum. The pretrained encoder is then fine-tuned in a multi-stage manner using limited labeled spectra and pseudo-labels. The representations learned in this semi-supervised framework show strong classification performance while using just 5% of the labeled data of a subset of the Bacteria-ID dataset.

However, these approaches primarily address the challenge of limited labeled Raman spectral data and do not explicitly take into account the variations arising from differences in instrumentation and experimental setups. Such variability can lead to significant distribution shifts, which can cause degradation of model performance during testing. Foundation models are designed to be quite robust to input distribution shifts by learning representations from large and diverse datasets. The Deep-spectral Component Filtering (DSCF) [54] is a foundation model that was developed through spectral component resolvable learning on over a million simulated and experimental spectra spanning several experiments and spectroscopic modalities (UV, IR and Raman). The authors showcased strong

performance of DSCF in multi-label classification with concentration estimation using simulated and experimental SERS spectra. However, its performance has not yet been evaluated on standard open-source Raman spectroscopy datasets.

The development of DSCF highlights the need for large-scale and diverse training data. Existing open-source Raman datasets are often restricted in size, chemical diversity or experimental variability. Creating large, curated experimental Raman spectral datasets that span multiple instruments, materials and measurement settings is key to developing a Raman-specific foundation model. These models could serve as a reusable backbone for a wide range of downstream tasks through lightweight fine-tuning using relatively small labeled datasets. This would significantly reduce annotation and training costs as the models would no longer need to be trained from scratch.

8 Conclusions

In this work, we presented a benchmark of five deep learning models for Raman spectra classification evaluated across three public datasets. These datasets capture different real-world challenges like domain shift due to acquisition variability (MLROD), multi-task clinical labeling (Bacteria-ID) and high-accuracy multi-category classification (API). All the models were evaluated using a unified experimental protocol to ensure fair comparison.

In MLROD, we observed a large disparity between the validation accuracies (99-100%) and test accuracies (74-80%) for all the models. The biggest degradation was on the dusty test subsets, implying brittleness to background interference and acquisition shift. In Bacteria-ID, isolate classification accuracy sits between 80-86%, while antibiotic treatment prediction is 96-98%. Finally for the API dataset, the models achieved near-ceiling accuracies between 99-100%. Overall, SANet demonstrated the best overall performance across the datasets, with the other models not too far behind.

The results of this benchmarking experiment have shown that classifying test samples that are in-distribution to the training dataset is significantly easier than test samples suffering from distribution shift due to changes in instruments and acquisition conditions, and additional contaminants. While this study benchmarks only five architectures and relies on minimal spectral pre-processing, it establishes a transparent and reproducible baseline for evaluating Raman spectra classifiers. We hope this benchmark will facilitate more rigorous comparisons, thereby enabling researchers to identify effective design choices and develop improved models in the future.

Author contributions

Adithya Sineesh conducted the Literature Survey, performed the benchmarking experiments and wrote the Benchmark Models, Results and Discussions Section.

Akshita Kamsali stylistically edited the Literature Survey along with authoring the Abstract, Introduction, Datasets, Methodology and Conclusion sections.

Acknowledgments

The authors would like to thank Dr. Avinash Kak for valuable discussions, guidance and access to computational resources that supported this work. The authors would also like to thank Dr. Rahul Deshmukh for his feedback on the manuscript.

Financial disclosure

None reported.

Conflict of interest

The authors declare no potential conflict of interests.

References

- [1] G. Berlanga, Q. Williams, and N. Temiquel. Convolutional neural networks as a tool for raman spectral mineral classification under low signal, dusty mars conditions. *Earth and Space Science*, 9(10):e2021EA002125, 2022.
- [2] T. Boucher, M. D. Dyar, and S. Mahadevan. Proximal methods for calibration transfer. *Journal of Chemometrics*, 31(4):e2877, 2017.
- [3] M. Chai, W. Hasi, X. Ming, S. Han, G. Fang, and Y. Bu. A novel method for rice identification: Coupling raman spectroscopy with fourier spectrum and analyzing with deep learning. *Journal of Food Composition and Analysis*, 136:106793, 2024.
- [4] L. Deng, Y. Zhong, M. Wang, X. Zheng, and J. Zhang. Scale-adaptive deep model for bacterial raman spectra identification. *IEEE Journal of Biomedical and Health Informatics*, 26(1):369–378, 2021.
- [5] J. Dong, M. Hong, Y. Xu, and X. Zheng. A practical convolutional neural network model for discriminating raman spectra of human and animal blood. *Journal of Chemometrics*, 33(11):e3184, 2019.
- [6] A. Dosovitskiy. An image is worth 16x16 words: Transformers for image recognition at scale. *arXiv preprint arXiv:2010.11929*, 2020.
- [7] F. Du, L. He, X. Lu, Y.-q. Li, and Y. Yuan. Accurate identification of living bacillus spores using laser tweezers raman spectroscopy and deep learning. *Spectrochimica Acta Part A: Molecular and Biomolecular Spectroscopy*, 289:122216, 2023.
- [8] J. Engel, J. Gerretzen, E. Szymańska, J. J. Jansen, G. Downey, L. Blanchet, and L. M. Buydens. Breaking with trends in pre-processing? *TrAC Trends in Analytical Chemistry*, 50:96–106, 2013.
- [9] M. Erzina, A. Trelin, O. Guselnikova, B. Dvorankova, K. Strnadova, A. Perminova, P. Ulbrich, D. Mares, V. Jerabek, R. Elashnikov, et al. Precise cancer detection via the combination of functionalized sers surfaces and convolutional neural network with independent inputs. *Sensors and Actuators B: Chemical*, 308:127660, 2020.
- [10] X. Fan, W. Ming, H. Zeng, Z. Zhang, and H. Lu. Deep learning-based component identification for the raman spectra of mixtures. *Analyst*, 144(5):1789–1798, 2019.
- [11] A. R. Flanagan and F. G. Glavin. Open-source raman spectra of chemical compounds for active pharmaceutical ingredient development. *Scientific Data*, 12(1):498, 2025.
- [12] M. T. Gebrekidan, C. Knipfer, and A. S. Braeuer. Refinement of spectra using a deep neural network: Fully automated removal of noise and background. *Journal of Raman Spectroscopy*, 52(3):723–736, 2021.
- [13] K. He, X. Zhang, S. Ren, and J. Sun. Deep residual learning for image recognition. In *Proceedings of the IEEE conference on computer vision and pattern recognition*, pages 770–778. IEEE, 2016.
- [14] C.-S. Ho, N. Jean, C. A. Hogan, L. Blackmon, S. S. Jeffrey, M. Holodniy, N. Banaei, A. A. Saleh, S. Ermon, and J. Dionne. Rapid identification of pathogenic bacteria using raman spectroscopy and deep learning. *Nature communications*, 10(1):4927, 2019.
- [15] J. Ho, A. Jain, and P. Abbeel. Denoising diffusion probabilistic models. *Advances in neural information processing systems*, 33:6840–6851, 2020.
- [16] J. Houston, F. G. Glavin, and M. G. Madden. Robust classification of high-dimensional spectroscopy data using deep learning and data synthesis. *Journal of Chemical Information and Modeling*, 60(4):1936–1954, 2020.
- [17] G. Huang, Z. Liu, L. Van Der Maaten, and K. Q. Weinberger. Densely connected convolutional networks. In *Proceedings of the IEEE conference on computer vision and pattern recognition*, pages 4700–4708, 2017.

[18] N. Ibtehaz, M. E. Chowdhury, A. Khandakar, S. Kiranyaz, M. S. Rahman, and S. M. Zughaiier. Ramannet: a generalized neural network architecture for raman spectrum analysis. *Neural Computing and Applications*, 35(25):18719–18735, 2023.

[19] T. Kirchberger-Tolstik, P. Pradhan, M. Vieth, P. Grunert, J. Popp, T. W. Bocklitz, and A. Stallmach. Towards an interpretable classifier for characterization of endoscopic mayo scores in ulcerative colitis using raman spectroscopy. *Analytical Chemistry*, 92(20):13776–13784, 2020.

[20] Y. E. Kok, A. Crisford, A. Parkes, S. Venkateswaran, R. Oreffo, S. Mahajan, and M. Pound. Classification of osteoarthritic and healthy cartilage using deep learning with raman spectra. *Scientific Reports*, 14(1):15902, 2024.

[21] O. C. Koyun, R. K. Keser, S. O. Sahin, D. Bulut, M. Yorulmaz, V. Yucesoy, and B. U. Toreyin. Ramanformer: A transformer-based quantification approach for raman mixture components. *ACS omega*, 9(22):23241–23251, 2024.

[22] A. Krizhevsky, I. Sutskever, and G. E. Hinton. Imagenet classification with deep convolutional neural networks. *Advances in neural information processing systems*, 25, 2012.

[23] B. Lafuente, R. T. Downs, H. Yang, and N. Stone. 1. the power of databases: The rruff project. In *Highlights in mineralogical crystallography*, pages 1–30. De Gruyter (O), 2015.

[24] J. Lai, M. Li, S. Chen, J. Long, Y. Chen, H. Lu, C. Zou, and Z. Zhang. Calibration transfer of deep learning models among multiple raman spectrometers via low-rank adaptation. *Analytical Chemistry*, 97(35):19009–19018, 2025.

[25] C. Lange, M. Altmann, D. Stors, S. Seidel, K. Moynahan, L. Cai, S. Born, P. Neubauer, and M. N. C. Bournazou. Deep learning for raman spectroscopy: Benchmarking models for upstream bioprocess monitoring. *Measurement*, page 118884, 2025.

[26] Y. LeCun, L. Bottou, Y. Bengio, and P. Haffner. Gradient-based learning applied to document recognition. *Proceedings of the IEEE*, 86(11):2278–2324, 2002.

[27] Y. Lin, Q. Zhang, H. Chen, S. Liu, K. Peng, X. Wang, L. Zhang, J. Huang, X. Yan, X. Lin, et al. Multi-cancer early detection based on serum surface-enhanced raman spectroscopy with deep learning: a large-scale case–control study. *BMC medicine*, 23(1):97, 2025.

[28] B. Liu, K. Liu, X. Qi, W. Zhang, and B. Li. Classification of deep-sea cold seep bacteria by transformer combined with raman spectroscopy. *Scientific Reports*, 13(1):3240, 2023.

[29] J. Liu, M. Osadchy, L. Ashton, M. Foster, C. J. Solomon, and S. J. Gibson. Deep convolutional neural networks for raman spectrum recognition: a unified solution. *Analyst*, 142(21):4067–4074, 2017.

[30] Y. Liu, Y. Gao, R. Niu, Z. Zhang, G.-W. Lu, H. Hu, T. Liu, and Z. Cheng. Rapid and accurate bacteria identification through deep-learning-based two-dimensional raman spectroscopy. *Analytica Chimica Acta*, 1332:343376, 2024.

[31] Z. Liu, Y. Lin, Y. Cao, H. Hu, Y. Wei, Z. Zhang, S. Lin, and B. Guo. Swin transformer: Hierarchical vision transformer using shifted windows. In *Proceedings of the IEEE/CVF international conference on computer vision*, pages 10012–10022, 2021.

[32] M. K. Maruthamuthu, A. H. Raffiee, D. M. De Oliveira, A. M. Ardekani, and M. S. Verma. Raman spectra-based deep learning: A tool to identify microbial contamination. *Microbiology-Open*, 9(11):e1122, 2020.

[33] H. M. Monavar, N. Afseth, J. Lozano, R. Alimardani, M. Omid, and J. Wold. Determining quality of caviar from caspian sea based on raman spectroscopy and using artificial neural networks. *Talanta*, 111:98–104, 2013.

[34] M. H. Mozaffari and L.-L. Tay. Convolutional neural networks for raman spectral analysis of chemical mixtures. In *2021 5th SLAAI International Conference on Artificial Intelligence (SLAAI-ICAI)*, pages 1–6. IEEE, 2021.

[35] M. H. Mozaffari and L.-L. Tay. Overfitting one-dimensional convolutional neural networks for raman spectra identification. *Spectrochimica Acta Part A: Molecular and Biomolecular Spectroscopy*, 272:120961, 2022.

[36] R. Nikzad-Langerodi and E. Andries. A chemometrician's guide to transfer learning. *Journal of Chemometrics*, 35(11):e3373, 2021.

[37] M. S. Primrose, J. Giblin, C. Smith, M. R. Anguita, and G. H. Weedon. One dimensional convolutional neural networks for spectral analysis. In *Algorithms, Technologies, and Applications for Multispectral and Hyperspectral Imaging XXVIII*, volume 12094, pages 98–108. SPIE, 2022.

[38] M. S. Primrose, G. H. Weedon, and J. Giblin. One-dimensional convolutional neural networks for raman spectral analysis. In *Chemical, Biological, Radiological, Nuclear, and Explosives (CBRNE) Sensing XXIV*, volume 12541, pages 151–160. SPIE, 2023.

[39] Y. Qi, D. Hu, M. Zheng, Y. Jiang, and Y. P. Chen. Deep learning assisted raman spectroscopy for rapid identification of 2d materials. *Applied Materials Today*, 41:102499, 2024.

[40] Y. Qin, J. Qiu, N. Tang, Y. He, and L. Fan. Deep learning analysis for rapid detection and classification of household plastics based on raman spectroscopy. *Spectrochimica Acta Part A: Molecular and Biomolecular Spectroscopy*, 309:123854, 2024.

[41] K. Rebrošová, M. Šiler, O. Samek, F. Růžička, S. Bernatová, V. Holá, J. Ježek, P. Zemánek, J. Sokolová, and P. Petráš. Rapid identification of staphylococci by raman spectroscopy. *Scientific reports*, 7(1):14846, 2017.

[42] P. Ren, R.-g. Zhou, and Y. Li. A self-supervised learning method for raman spectroscopy based on masked autoencoders. *Expert Systems with Applications*, page 128576, 2025.

[43] Y. Roggo, K. Degardin, and P. Margot. Identification of pharmaceutical tablets by raman spectroscopy and chemometrics. *Talanta*, 81(3):988–995, 2010.

[44] K. Simonyan and A. Zisserman. Very deep convolutional networks for large-scale image recognition, 2015.

[45] J. Sjöberg, N. Siminea, A. Păun, A. Lita, M. Larion, and I. Petre. Radar: Raman spectral analysis using deep learning for artifact removal. *Advanced Optical Materials*, page 2500736, 2025.

[46] Z. Sun and Z. Wang. Semiraman: A self-supervised contrastive representation learning-based framework for semi-supervised raman spectral identification of pathogenic bacteria. *Spectrochimica Acta Part A: Molecular and Biomolecular Spectroscopy*, page 127356, 2025.

[47] C. Szegedy, V. Vanhoucke, S. Ioffe, J. Shlens, and Z. Wojna. Rethinking the inception architecture for computer vision. In *Proceedings of the IEEE conference on computer vision and pattern recognition*, pages 2818–2826, 2016.

[48] R. Ullah, S. Khan, Z. Ali, H. Ali, A. Ahmad, and I. Ahmed. Evaluating the performance of multilayer perceptron algorithm for tuberculosis disease raman data. *Photodiagnosis and Photodynamic Therapy*, 39:102924, 2022.

[49] A. Umprecht, V. F. Diaz, B. Hüpfl, B. Kozma, A. Schwaighofer, M. Henson, R. Nikzad-Langerodi, and O. Spadiut. Unsupervised optimization of spectral pre-processing selection to achieve transfer of raman calibration models. *Measurement*, 255:117906, 2025.

[50] A. Vaswani, N. Shazeer, N. Parmar, J. Uszkoreit, L. Jones, A. N. Gomez, Ł. Kaiser, and I. Polosukhin. Attention is all you need. *Advances in neural information processing systems*, 30, 2017.

[51] R. t. Vulchi, V. Morgunov, R. Junjuri, and T. Bocklitz. Artifacts and anomalies in raman spectroscopy: A review on origins and correction procedures. *Molecules*, 29(19):4748, 2024.

[52] Y. Wang, L. Xu, L. Shang, H. Peng, K. Liu, X. Bao, X. Tang, P. Liang, Y. Wang, M. Zheng, et al. Deep learning-assisted raman spectroscopy for rapid lactic acid bacteria identification at the colony level. *Spectrochimica Acta Part A: Molecular and Biomolecular Spectroscopy*, 344:126662, 2026.

[53] Z. Wang, Y. Li, J. Zhai, S. Yang, B. Sun, and P. Liang. Deep learning-based raman spectroscopy qualitative analysis algorithm: A convolutional neural network and transformer approach. *Talanta*, 275:126138, 2024.

[54] B. Xue, X. Bi, Z. Dong, Y. Xu, M. Liang, X. Fang, Y. Yuan, R. Wang, S. Liu, R. Jiao, et al. Deep spectral component filtering as a foundation model for spectral analysis demonstrated in metabolic profiling. *Nature Machine Intelligence*, 7(5):743–757, 2025.

[55] G. Yin, L. Li, S. Lu, Y. Yin, Y. Su, Y. Zeng, M. Luo, M. Ma, H. Zhou, L. Orlandini, et al. An efficient primary screening of covid-19 by serum raman spectroscopy. *Journal of Raman Spectroscopy*, 52(5):949–958, 2021.

[56] S. Yu, H. Li, X. Li, Y. V. Fu, and F. Liu. Classification of pathogens by raman spectroscopy combined with generative adversarial networks. *Science of The Total Environment*, 726:138477, 2020.

[57] Z. Zhang, Y. Liu, C. Chen, X. Lv, and C. Chen. Unsupervised domain adaptation with raman spectroscopy for rapid autoimmune disease diagnosis. *Sensors*, 25(19):6186, 2025.

[58] Z. Zhao, Z. Liu, M. Ji, X. Zhao, Q. Zhu, and M. Huang. Conincedep: A novel deep learning method for component identification of mixture based on raman spectroscopy. *Chemometrics and Intelligent Laboratory Systems*, 234:104757, 2023.

[59] B. Zhou, Y.-K. Tong, R. Zhang, and A. Ye. Ramannet: a lightweight convolutional neural network for bacterial identification based on raman spectra. *RSC advances*, 12(40):26463–26469, 2022.